Supporting Information

The Ever-Evolving Active Site: Transformation of Single Atoms to Extended Structures during Rh-catalyzed Reverse Water-Gas Shift Reaction

Greg Barber[a$], Xiaobo Chen[b,c$], Anastassiya Khan[d], Jake Heinlein[e], Sabrina M. Gericke[b], Meng Li[b], Dmitri Zakharov[b], Judith Yang[b,c], Ashley R. Head[b], Matteo Cargnello[e], Robert M. Rioux[a,f], Simon R Bare[d]

[a] Department of Chemical Engineering, Pennsylvania State University, University Park, Pennsylvania, 16802, United States

[b] Center for Functional Nanomaterials, Brookhaven National Laboratory, Upton, New York 11973, United States

[c] Department of Chemical and Petroleum Engineering, University of Pittsburgh, Pittsburgh, Pennsylvania 15261, United States

[d] SSRL, SLAC National Accelerator Laboratory, Menlo Park, California, 94025, United States

[e] Department of Chemical Engineering, Stanford University, Stanford, California 94305, United States

[f] Department of Chemistry, Pennsylvania State University, University Park, Pennsylvania 16802, United States

[$]These authors contributed equally to the work

Section 1. Analysis of the $Rh/rTiO_2$ (CS/NP)

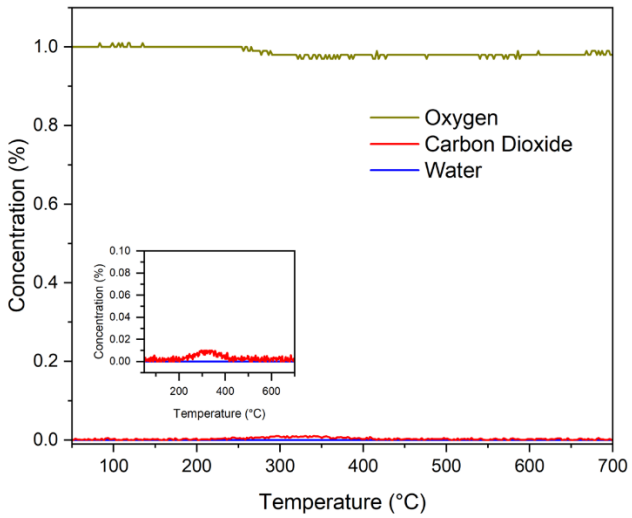

Fig S1. TPO Conditions: 250 mg of 0.5% $Rh/rTiO_2$ (CS/NP) were loaded into the reactor while flowing 1% O_2 in Ar at 20 sccm. The temperature was ramped to 700 °C at a rate of 10 °C/min.

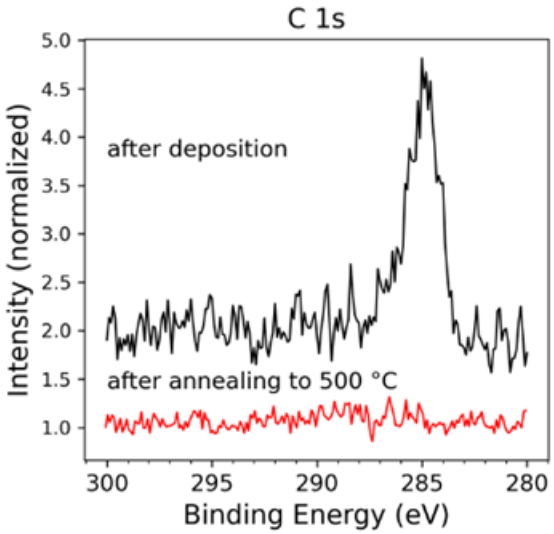

Fig. S2. C 1s spectra of Rh colloidal NPs on TiO_2 after deposition of the NPs (top spectrum) and after annealing in O_2 at 500 °C for 3 h (bottom spectrum). After the deposition, a clear carbon peak is visible but after annealing in O_2, no carbon can be detected in the XPS spectrum, showing that the calcination step removed the carbon.

Section 2. Transmission electron microscopy characterization of $Rh/rTiO_2$ catalysts

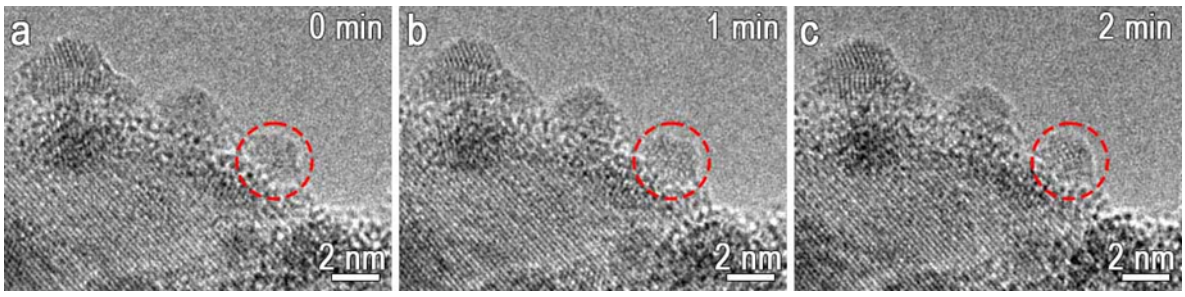

Fig. S3. In situ HRTEM images showing Rh nanoparticles exposed to continuous electron-beam irradiation at a dose rate of approximately ~$4.2\times10^5 e$ nm^{-2} s^{-1}, indicating beam-induced rearrangement of atomic columns. The dashed red circles highlight the progressive crystallization of Rh nanoparticles from a disordered to an ordered atomic arrangement. This experiment confirms that 0.5 s exposure to be free from beam-induced effects.

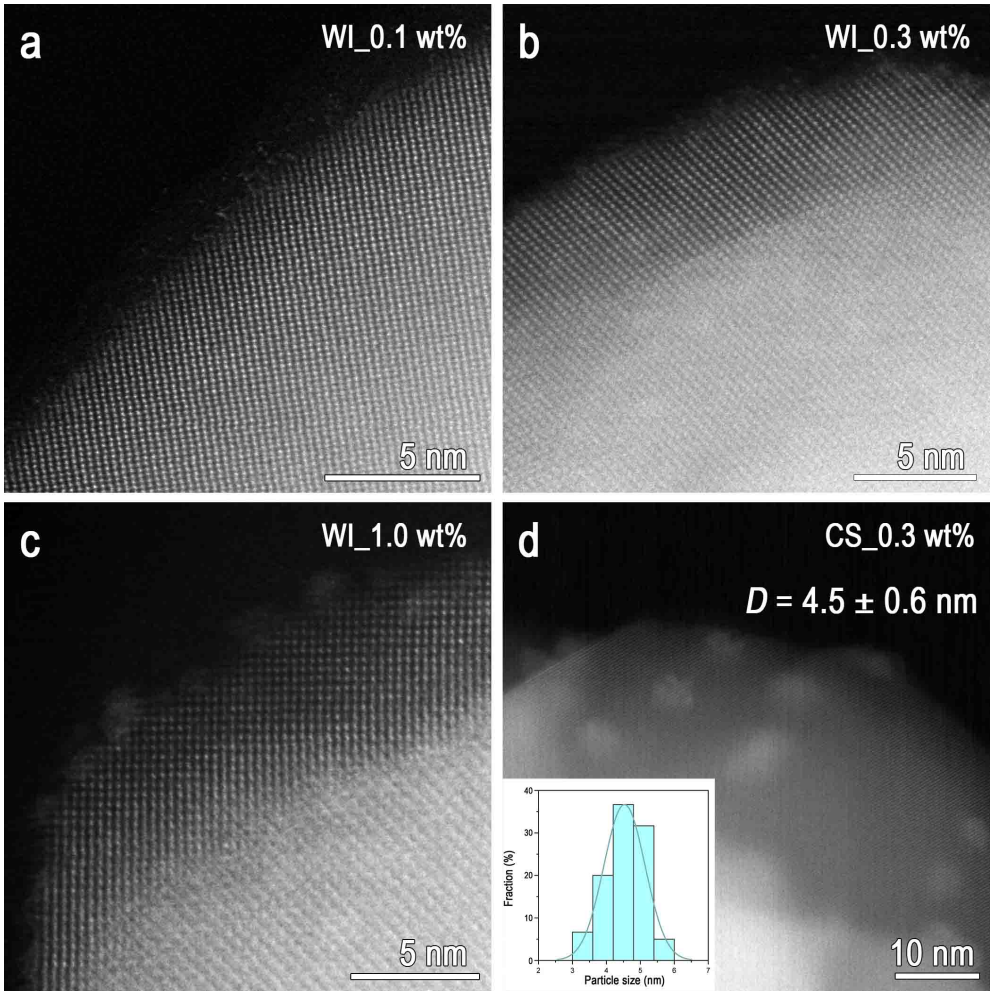

Fig. S4. High-angle annular dark-field scanning transmission electron microscopy (HAADF-STEM) imaging of fresh Rh/rTiO_2 catalysts with different loading: (a) 0.1 wt. % Rh (WI), (b) 0.3 wt. % Rh (WI), (c) 1 wt. % Rh (WI), and (d) 0.3 wt. % Rh (CS/NP). The inset is the particle size distribution of 0.3 wt. % Rh/rTiO_2 (CS/NP).

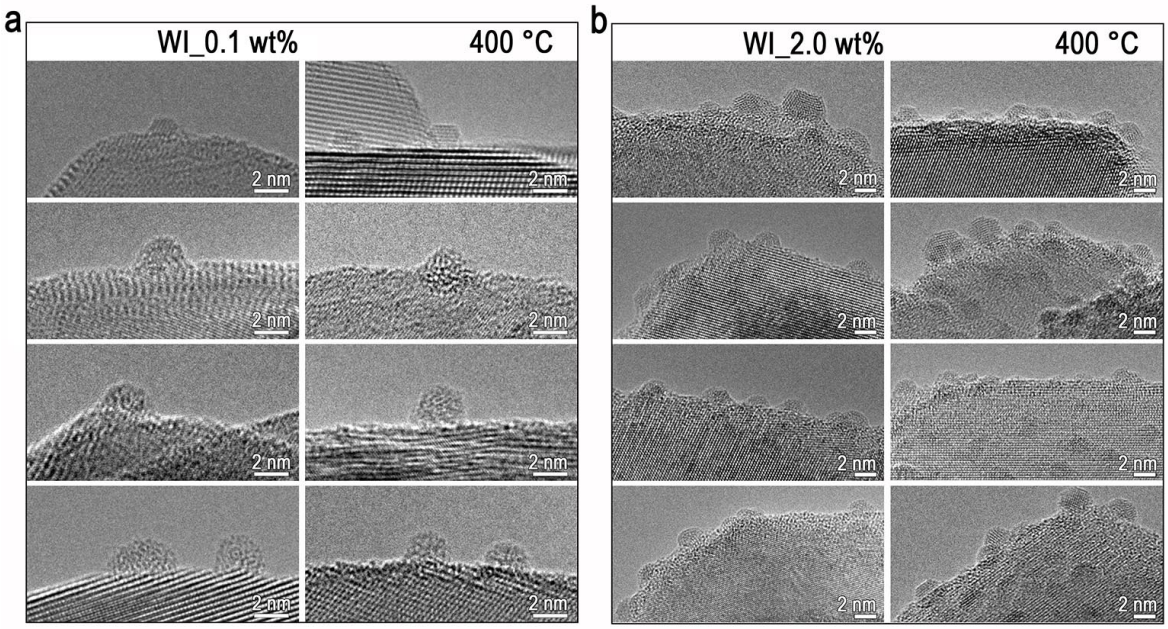

Fig. S5. High resolution TEM imaging of post-reaction Rh/rTiO_2 catalysts at 400°C with different Rh loading: (a) 0.1 wt. % Rh (WI) and (b) 2.0 wt. % Rh (WI), displaying disordered structure and irregular morphology of Rh nanoparticles.

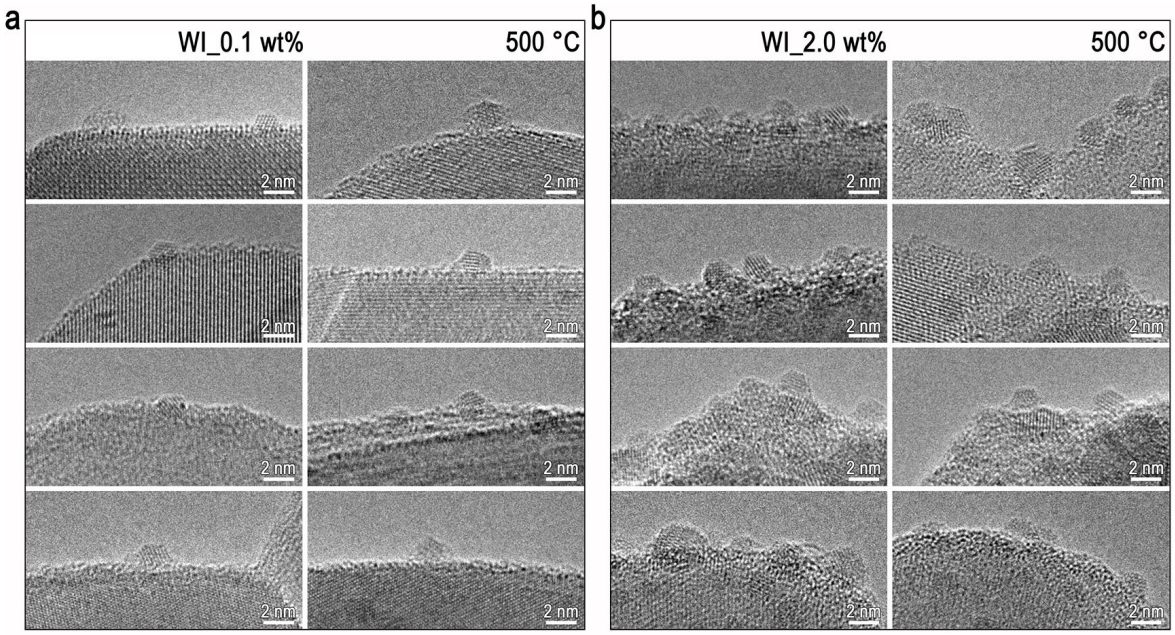

Fig. S6. High resolution TEM images of post-reaction $Rh/rTiO_2$ catalysts at 500°C with different loading: (a) 0.1 wt. % Rh (WI) and (b) 2.0 wt. % Rh (WI).

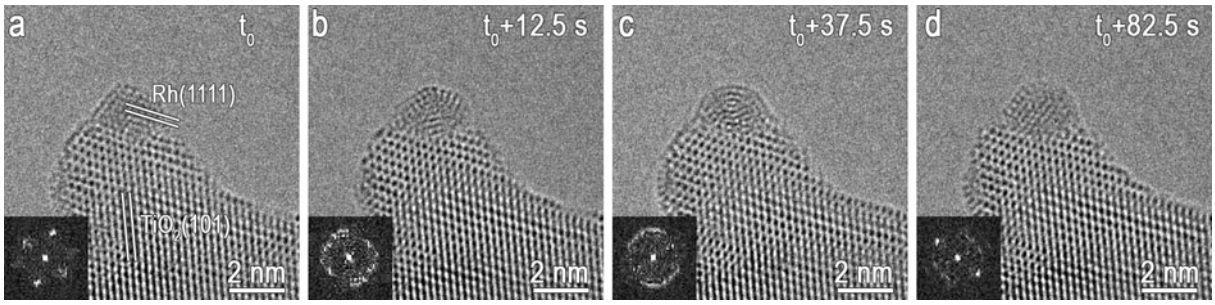

Fig S7. In-situ ETEM observations of structural evolution of Rh/TiO_2 during RWGS reaction. a-d, Real-time HRTEM images showing the reversible structural transformation of Rh nanoparticles from a well-ordered crystalline state to a disordered structure and subsequently back to a crystalline phase under exposure to gas mixture of ~ 3×10^{-3} Torr H_2 and 10^{-2} Torr CO_2 at 500 °C.

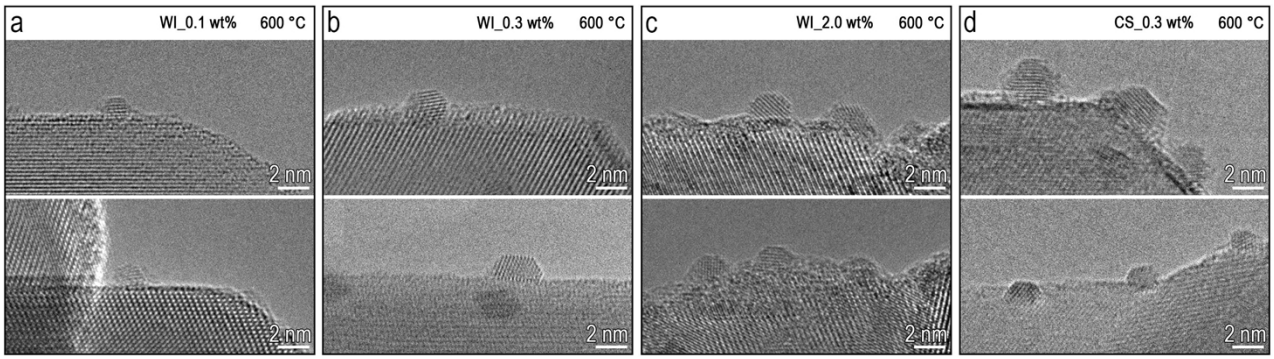

Fig. S8. Additional HRTEM imaging of post-reaction $Rh/rTiO_2$ catalysts at 600°C with different loading: (e) 0.1 wt. % Rh (WI), (f) 0.3 wt. % Rh (WI), (g) 2 wt. % Rh (WI), and (h) 0.3 wt. % Rh (CS/NP), showing the well-crystallized and faceted Rh NPs.

Section 3. X-ray Photoelectron Spectroscopy (XPS)

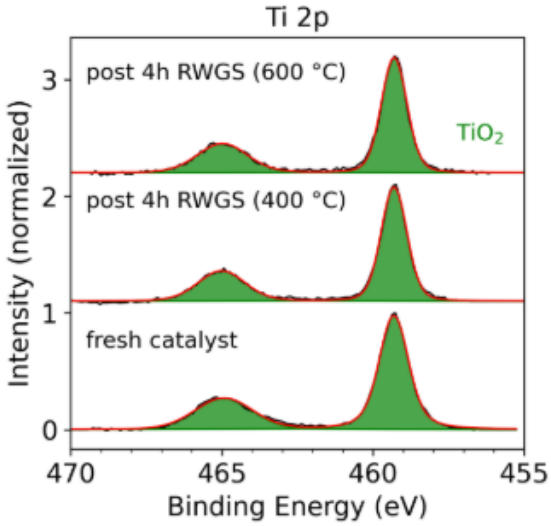

Fig. S9. *In situ* XPS measurements of the Ti 2p core level of the 2.0 wt.% WI catalysts as synthesized (fresh catalyst) and after 1 mbar O_2 at 400°C for 30 min with subsequent heating in 1 mbar of a H_2/CO_2 gas mixture (3:1 ratio) at the indicated temperatures. The spectra are background subtracted and normalized to the intensity of the main peak. The Ti $2p_{3/2}$ position was used for binding energy calibration of all spectra by shifting to 459.3 eV. The spectra are background subtracted and normalized to the intensity of the main peak.

XPS measurements were performed to determine the oxidation state of the Rh catalysts. Fig. 5i in the main manuscript shows the Rh 3d spectra of the 2.0 wt.% Rh/rTiO_2 (WI) collected under several conditions. Figure S4 shows the corresponding Ti 2p core levels. The bottom spectrum in Figs. 5i and S4 corresponds to the post-synthesis catalyst measured in UHV. The Rh $3d_{5/2}$ peak appears at 310.3 eV, consistent with Rh_2O_3, demonstrate the as-prepared catalyst is oxidized.[1] To evaluate the oxidation state under reaction conditions, each catalyst was first oxidized in 1 mbar O_2 at 400°C for 30 min to remove residual surface carbon. The sample was then exposed to 1 mbar of a H_2/CO_2 gas mixture (3:1 ratio) and heated to 400°C or 600°C. Each sample was held at the respective temperature for 4 h before cooling to room temperature for XPS analysis. After the RWGS treatment, both samples exhibit substantial reduction. The catalyst reacted at 400°C has a Rh $3d_{5/2}$ peak at 307.5 eV, while the catalyst reacted at 600°C shifts to a slightly lower energy of 307.3 eV. These lower binding energies are characteristic of metallic Rh.[1,2] The binding energy shift between the different temperatures suggests higher treatment temperatures lead to Rh nanoparticles that behave more like bulk Rh, which may reflect increased particle size or higher crystallinity.[2] Furthermore, the Rh peaks in the catalyst reacted at 600°C are noticeably narrower

than those in for the catalyst reacted at 400°C, which may indicate increased structural ordering or higher crystallinity of the rhodium at elevated temperature. As shown by the consistent Ti 2p spectra in Figure S4, no Ti^{3+} is detected at lower binding energy. To investigate potential SMSI encapsulation, the intensity of the Rh 3d was divided by the Ti 2p intensity: 0.39 for the 400°C sample and 0.38 for the 600 °C sample. The consistent values support a lack of encapsulation, which would attenuate the Rh 3d signal.

Section 4. Deconvolution of DRIFTS spectra of CO adsorption on 0.3 wt. % $Rh/rTiO_2$ (CS/NP) after different annealing treatments

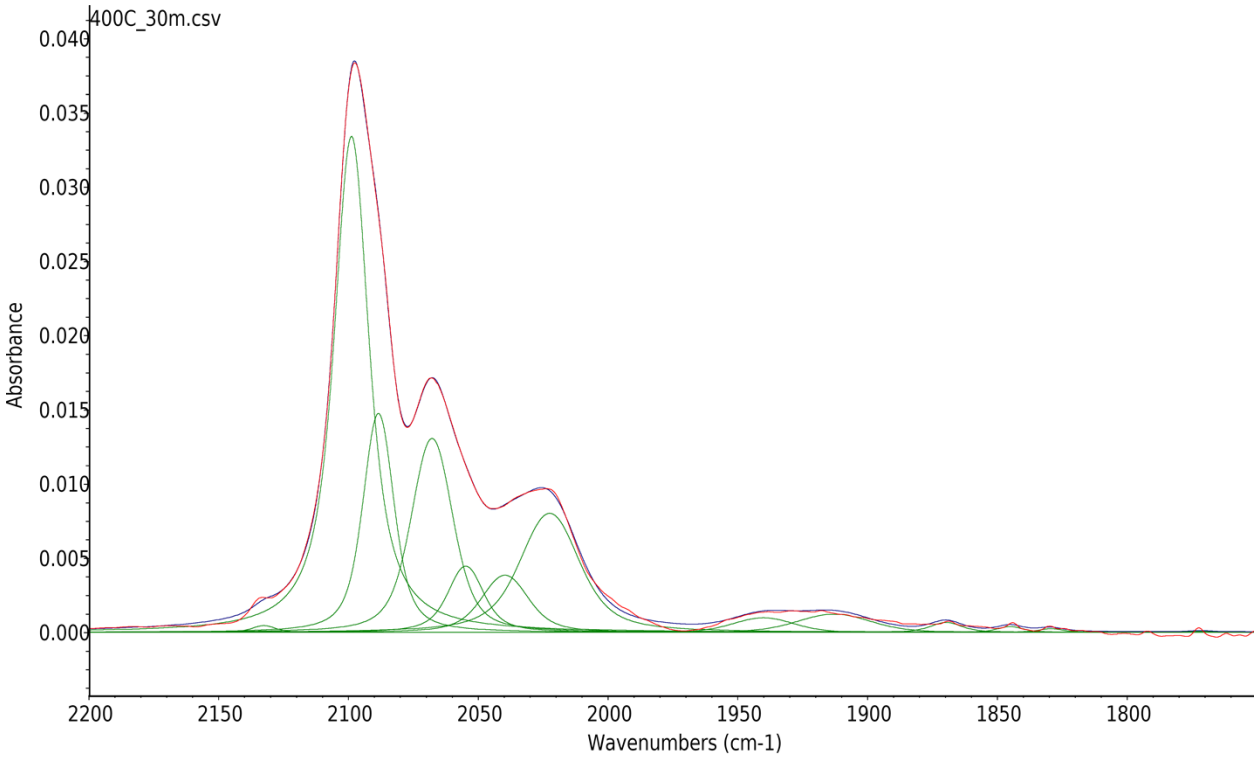

Fig. S10. CO DRIFTS and deconvoluted peaks of 0.3 wt. % (CS/NP) $Rh/rTiO_2$ sample annealed at 400°C for 30 min. Experimental spectrum in red, deconvoluted peaks using default parameters in OMNIC (ThermoFisher) in green, and the sum of deconvoluted peaks in black. No software forcings were used for peak locations and Voigt parameters. The complete deconvolution process details are in the Experimental section.

Table S1. Table of deconvoluted CO DRIFTS peaks using OMNIC software from 1750-2200 cm^{-1} for the data and sample annealed at 400 °C for 30 min shown in Fig. S8. FWHH is Gaussian Full-Width at Half-Height (FWHH) and Other is Lorentzian FWHH to Voigt Function.

Peak Type	Center X	Height	FWHH	Other	Area
Voigt	2132.566	0.0005	6.603	6.451	0.0066
Voigt	2098.821	0.0334	6.741	12.954	0.7826
Voigt	2088.427	0.0148	9.526	7.412	0.2731
Voigt	2067.779	0.0131	13.879	8.343	0.3134
Voigt	2054.789	0.0045	10.461	9.331	0.0974
Voigt	2039.685	0.0039	15.306	9.876	0.1049
Voigt	2022.454	0.008	18.025	14.611	0.2865
Voigt	1940.096	0.001	23.743	6.42	0.0313
Voigt	1912.876	0.0012	28.029	9.476	0.0488
Voigt	1869.695	0.0007	8.45	9.175	0.0132
Voigt	1845.015	0.0004	7.17	7.328	0.0062
Voigt	1829.362	0.0002	7.256	7.257	0.0038
Voigt	1771.557	0.0001	7.232	6.977	0.0012

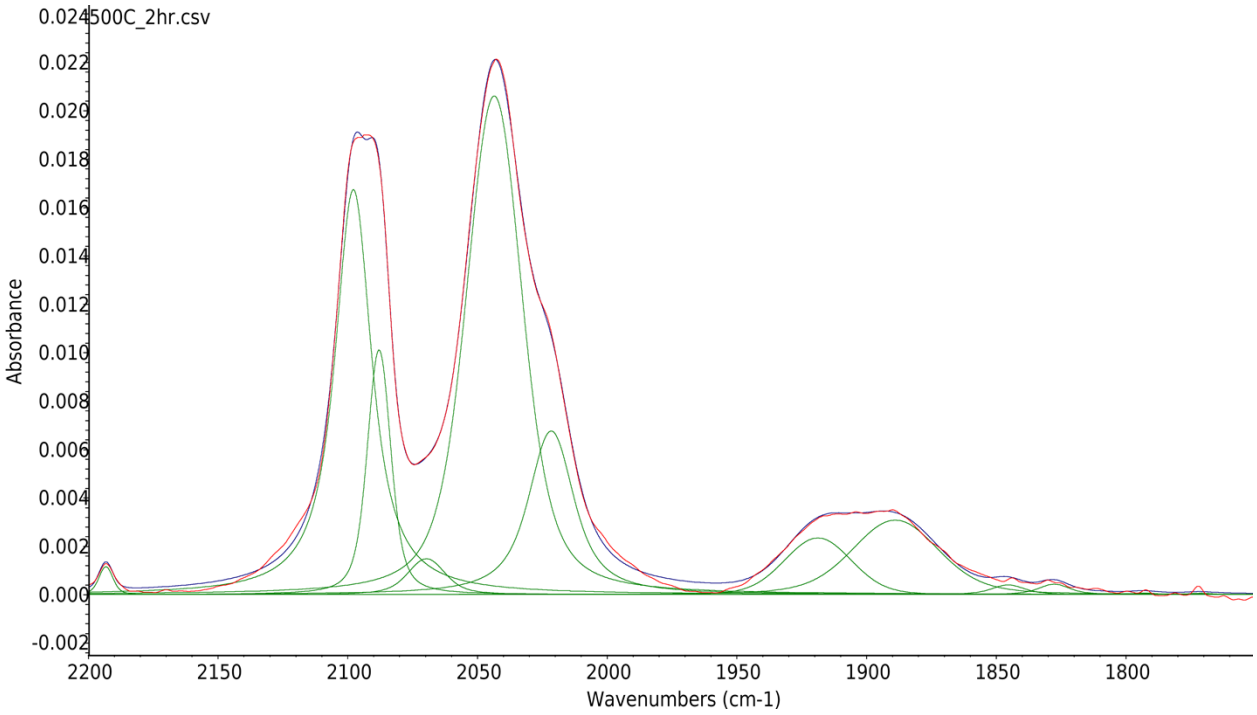

Fig. 11. CO DRIFTS and deconvoluted peaks of 0.3 wt. % (CS/NP) Rh/rTiO_2 sample annealed at 500 °C for 2 h. Experimental spectrum in red, deconvoluted peaks using default parameters in OMNIC (ThermoFisher) in green, and the sum of deconvoluted peaks in black. No software forcings were used for peak locations and Voigt parameters. The complete deconvolution process details are in the Experimental section.

Table S2. Table of deconvoluted CO DRIFTS spectra using OMNIC software from 1750-2200 cm^{-1} for the data and sample annealed at 500°C for 2 h in Fig. S9. FWHH is Gaussian Full-Width at Half-Height (FWHH) and Other is Lorentzian FWHH to Voigt Function.

Peak Type	Center X	Height	FWHH	Other	Area
Voigt	2193.236	0.0011	5.034	2.317	0.009
Voigt	2097.86	0.0167	4.644	15.505	0.4306
Voigt	2087.923	0.0101	7.772	4.834	0.1379
Voigt	2069.639	0.0015	12.237	7.81	0.0321
Voigt	2043.509	0.0206	18.664	11.348	0.6675
Voigt	2021.537	0.0068	10.04	15.611	0.2009
Voigt	1918.74	0.0023	28.365	3.631	0.0793
Voigt	1888.888	0.0031	32.671	11.385	0.144
Voigt	1845.387	0.0004	8.942	9.555	0.0082
Voigt	1827.633	0.0004	8.456	8.937	0.0083
Voigt	1792.95	0.0001	7.619	7.617	0.0011
Voigt	1771.221	0.0001	7.623	7.61	0.001

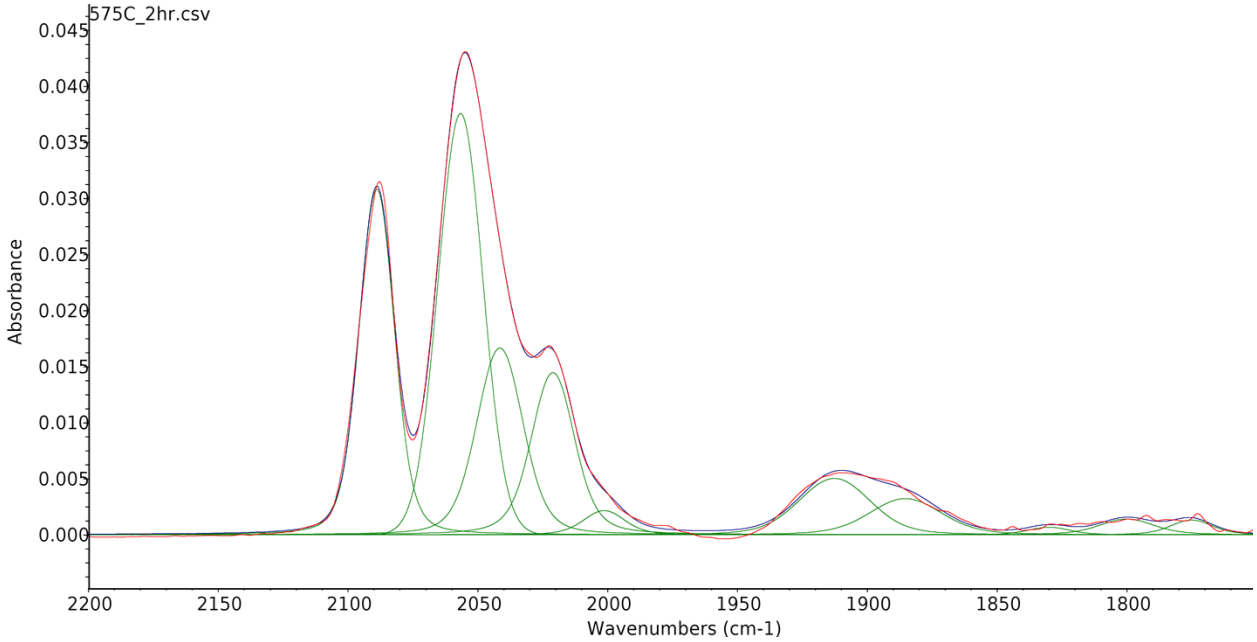

Fig. S12. CO DRIFTS and deconvoluted peaks of 0.3 wt. % (CS/NP) Rh/rTiO_2 sample annealed at 575°C for 2 h. Experimental spectrum in red, deconvoluted peaks using default parameters in OMNIC (ThermoFisher) in green, and the sum of deconvoluted peaks in black. No software forcings were used for peak locations and Voigt parameters. The complete deconvolution process details are in the Experimental section.

Table S3. Table of deconvoluted CO DRIFTS peaks using OMNIC software from 1750-2200 cm^{-1} for each of the samples annealed at 575 °C for 2 h in Fig. S10. FWHH is Gaussian Full-Width at Half-Height (FWHH) and Other is Lorentzian FWHH to Voigt Function.

Peak Type	Center X	Height	FWHH	Other	Area
Voigt	2088.915	0.0308	13.847	3.625	0.5715
Voigt	2056.655	0.0376	20.241	0.008	0.8107
Voigt	2041.499	0.0167	17.998	5.197	0.4103
Voigt	2021.078	0.0145	15.796	6.435	0.3429
Voigt	2001.348	0.0022	15.011	6.592	0.0497
Voigt	1912.631	0.005	28.363	6.975	0.1883
Voigt	1885.271	0.0032	27.372	9.412	0.1259
Voigt	1830.061	0.0007	14.855	7.368	0.0159
Voigt	1800.025	0.0014	18.477	10.721	0.0442
Voigt	1775.061	0.0013	14.855	7.368	0.0312

References

1. G. Munuera, A. R. Gonzalez-Elipe, J. P. Espinos, A. Navio. XPS characterization of oxygenated species in TiO2 and Rh/TiO2 photocatalysts. Journal of Molecular Structure 143 (1986) 227-230.
2. L. Óvári, J. Kiss. Growth of Rh nanoclusters on TiO2(110): XPS and LEIS studies. Applied Surface Science 252 (2006) 8624-8629.